opening angle θ and the observed daughter filament radius a (estimated from the amount of diffraction of each filament after exit from the cell), versus sodium density N. The theoretical half-opening angle θ [Eq. (10)] and the theoretical filament radius[6],

$$a = 0.61\lambda(2\pi N|\alpha'|)^{-1/2}, \quad (11)$$

derived by equating the effects of diffraction and self-focusing, are also plotted in Fig. 3(b), with $|\alpha'(\Delta\nu)|$ being taken as 10^{-18} cm^{-3}.[7] Reasonable agreement is obtained, especially at higher densities, when the observed values of θ and a follow the predicted $N^{1/2}$ and $N^{-1/2}$ dependence very closely. The poorer agreement at lower density is not completely understood, but may be due to too large filament size or too weak repulsion so that the daughter beams have not reached the asymptotic opening angle yet before they exit from the cell. The data of Fig. 3 are for zero applied magnetic field; applying a transverse magnetic field diminishes θ as expected.

*This work was supported by the U. S. Air Force Office of Scientific Research.

[1]O. Svelto, in *Progress in Optics*, edited by E. Wolf (North-Holland, Amsterdam, 1974), Vol. 12, p. 1.

[2]S. A. Akhamonv, A. P. Sukhorukov, and R. V. Khokhlov, Usp. Fiz. Nauk 93, 19 (1967) [Sov. Phys. Usp. 93, 609 (1968)].

[3]Y. R. Shen, Rev. Mod. Phys. 48, 1 (1976).

[4]D. Grischkowsky, Phys. Rev. Lett. 24, 866 (1970).

[5]J. E. Bjorkholm and A. Ashkin, Phys. Rev. Lett. 32, 129 (1974).

[6]A. Javan and P. L. Kelley, IEEE J. Quantum Electron. QE-2, 470 (1966).

[7]B. S. Mathur, H. Y. Tang, and W. Happer, Phys. Rev. A 2, 648 (1970).

[8]G. A. Askar'yan, Zh. Eksp. Teor. Fiz 42, 1567 (1962) [Sov. Phys. JETP 15, 1088 (1962)].

[9]V. I. Bespalov and V. I. Talanov, Pis'ma Zh. Eksp. Teor. Fiz. 3, 471 (1966) [JETP Lett. 3, 307 (1966)].

[10]A. J. Campillo, S. L. Shapiro, and B. R. Suydam, Appl. Phys. Lett. 23, 628 (1973).

Space-Time Implosion Characteristics of Laser-Irradiated Fusion Targets*

D. T. Attwood, L. W. Coleman, M. J. Boyle, J. T. Larsen, D. W. Phillion, and K. R. Manes
Lawrence Livermore Laboratory, University of California, Livermore, California 94550
(Received 8 November 1976)

An x-ray pinhole camera is coupled to an x-ray streak camera for detailed measurements of the implosion of laser fusion targets. Simultaneous spatial and temporal resolutions of 6 μm and 15 psec are attained. Resultant R and t implosion diagrams show time-dependent implosion velocites in the range of $(3-4)\times 10^7$ cm/sec.

Experiments designed to study laser-driven implosions of glass microshells are underway in several laboratories worldwide. The ultimate goal of these experiments is to drive the encapsulated deuterium-tritium fuel to a sufficiently high density and temperature that the resultant thermonuclear reaction produces a net gain.[1] In preliminary experiments it has been shown that modest compressions are achieved[2,3] and that the resulting fusion reactions are of thermonuclear origin.[4] It is important that these early experiments be understood in sufficient detail that future experiments can be accurately designed. Because of the high densities and temperatures involved, x-ray emission from the compressed target provides a primary souce of data regarding dynamics of the implosion process. A typical implosion experiment involves an approximately 100-μm-initial-diameter target which implodes to a fraction of its original size on a time scale of roughly 100 psec. The x-ray data must therefore be resolved spatially to microns and temporally to picoseconds in order to provide direct data describing the heating and implosion processes. However, diagnostics available to date have not had the capability of simultaneously providing the required space-time resolutions. Time-integrated x-ray-imaging studies provide spatially resolved photographs showing target compression.[2,3] Spatially integrated streak-camera studies provide temporally resolved x-ray spectral signals interpretable in terms of implosion times.[5] In this Letter, we report the first temporally resolved x-ray images of laser-compressed targets with sufficient resolutions to follow the implosion process continuously. The re-

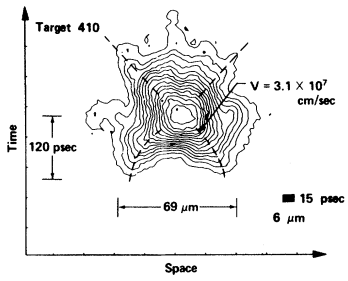

FIG. 1. Space-time isodensity contours for a two-sided target irradiation experiment. Density contour interval is 0.2, increasing monotonically toward the center of the x-ray pinhole streak record. Initial target had a 69-μm diameter, a 0.44-μm wall, and a DT fill of 1.67 mg/cm^3. Upon two-sided laser irradiation with 14.2- and 13.3-J, 64-psec pulses, the target compressed and produced 1×10^6 neutrons. (Target shot no. 76070805).

sultant space-time emission characteristics provide directly observable, time-dependent, implosion velocities. Because these velocities are sensitive to the mechanism and efficiency of energy transport from the corona region, their detailed measurement provides a basis for testing the validity of our physical models of the implosion process.

In these recent experiments, glass microshell targets with diameters in the range 60–130 μm, with wall thicknesses of typically 0.5 μm and deuterium-tritium (DT) fills of approximately 2 mg/cm^3, were irradiated by 1.06-μm, 70-psec (full width at half-maximum) pulses from the 0.4-TW Janus laser system.[6] Two-sided target illumination was accomplished with ellipsoidal focusing mirrors (with a numerical aperture of 0.99).[7] Images of the imploding targets, in their

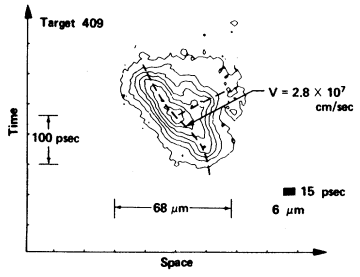

FIG. 2. Same as Fig. 1, for a single-sided target irradiation. Note that implosion is from one side only, that it converges near target center, and that disassembly is two-sided, albeit asymmetric. The initial target had a 68-μm diameter, 0.57-μm wall, and a DT fill of 1.82 mg/cm^3. Upon laser irradiation with a 15.3-J, 70-psec pulse, it produced 2×10^5 neutrons. (Target shot no. 76070906.)

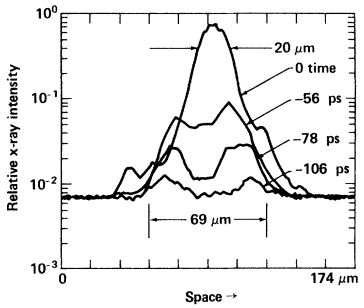

FIG. 3. Spatial contours of x-ray emission showing the implosion of target 410 (Fig. 1) at various times.

own x-ray emission, were formed with a 6-μm-diam, 50×-magnification pinhole camera, and recorded with our 15-psec x-ray streak camera.[5] The pinhole alignment procedure and details of the specially fabricated pinholes are described by Attwood, Weinstein, and Wuerker.[8] With a diameter of the target image aligned on the streak-camera entrance slit, a properly timed streak record provides a space-time implosion history of the irradiated target. Representative data are shown in Figs. 1 and 2 for two-sided and one-sided target irradiations, respectively. A 125-μm-thick beryllium foil was used to filter x-rays (2–3 keV) and to protect the tantalum-glass pinhole material.[9] Figures 1 and 2 show isodensity film contours increasing monotonically in density steps of 0.2. Shaded blocks in the lower right-hand corner of each figure show the approximate space-time resolutions of 6 μm and 15 psec.

Several features of the observed density contours are immediately evident in Figs. 1 and 2. One observes, for instance, that the two-sided irradiation of target 410 led to an approximately symmetric target implosion and disassembly. On the other hand, single-sided irradiation of target 409 produced a one-sided implosion, converging near the target center, followed by a two-sided but asymmetric disassembly. Note that beyond the period of peak x-ray emission, the contours appear to coast towards the unirradiated side, as one would expect from conservation of momentum arguments. Target 410 (Fig. 1) is representative of our two-sided irradiation experiments with large absorbed power (or energy) per unit target mass (6 GW/ng and 0.4 J/ng for a 65-psec pulse).[10] Considering target No. 410 further, properties of the streak recording film are removed by use of a film calibration curve (D vs $\ln E$) to convert the film density contours of Fig. 1 to relative x-ray exposure. Spatial profiles of relative x-ray intensity are then obtained at various times as seen

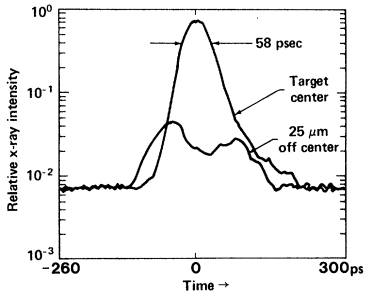

FIG. 4. Temporal profiles showing the history of x-ray emission from the center of target 410 and from a position 25 μm off center.

in Fig. 3; temporal profiles at two spatial positions are shown in Fig. 4. The spatial profiles of Fig. 3 show that at an early time (−106 psec) peak x-ray emission emanates from positions near but inside the initial target wall position. At a later time (−78 psec) x-ray emission has moved inward and become more intense. Still later (−56 psec) the oppositely directed fronts begin to coalesce; and finally they converge to produce an intense peak of x-ray emission at the target center. The temporal profiles of Fig. 4 show the x-ray-emission history at the target center and at a position 25 μm off center. Note that the latter displays a two-humped behavior—one corresponding to the emission front passing during implosion, and a

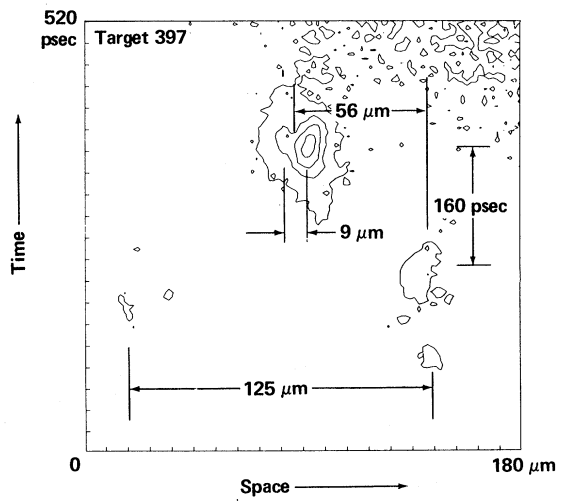

FIG. 5. Space-time isodensity contours for two-sided irradiation of a larger-radius, more massive target in which power absorbed per unit target mass is low (1.1 GW/ng). The initial target had a 125-μm diameter, a 0.86-μm wall, and a DT fill of 0.99 mg/cm^3. Upon two-sided laser irradiation with 17.8- and 17.7-J, 79-psec pulses, it produced 5×10^5 neutrons. (Target shot no. 76073002.)

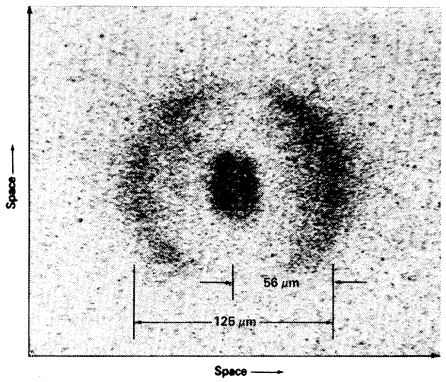

FIG. 6. Two-dimensional x-ray microscope image (time integrated) for the same target experiment described in Fig. 5.

second during disassembly.

For larger-diameter, more massive targets than discussed above, x-ray emission is reduced. Furthermore, the numerical simulations predict sharp spatial and temporal decays of emission as the shell explodes inward and outward decreasing the density in the emitting region. Density and, concomitantly, emission again rise as the inwardly converging portions of the shell stagnate near the target center. Results for a massive, large-diameter case (1.1 GW/ng, 0.09 J/ng, and 79 psec) are shown in Figs. 5 and 6. Figure 5 shows the spatially and temporally resolved implosion of this 125-μm-diam, 0.86-μm-thick wall, 0.99-mg/cm^3 DT-filled target. The film density contours show that the x-ray intensity was relatively weak, initially emanated from opposite sides of the target periphery, decreased below detectability because of density decay, and rose again 160 psec later to a spatially separated target core. Implosion velocities observed here are approximately 3.5×10^7 cm/sec. The corresponding x-ray microscope image (two-dimensional, time-integrated) is shown in Fig. 6 for comparison. It shows complementary features: a ring of emission at the initial wall position and a somewhat off-center, split target core.

The dashed lines in Figs. 1 and 2 trace the propagation of peak x-ray emission towards the target center, and can be interpreted as characteristics of the implosion process, the slopes of which are velocities in these space-time diagrams. Velocity values near peak compression are shown in both figures; these are not necessarily material velocities. However, two-dimensional numerical simulations[11] permit us to separate the ef-

fects of irradiation geometry and density-temperature profiles so that the relation between these velocities is well understood. Because peak x-ray emission emanates from the most dense region of the shell, the final values are not greatly different. These calculations also show that the shell is exploded by superthermal electrons to a fuel-pusher interface velocity approaching 10^7 cm/sec, and is then driven by thermal-electron pressure at approximately constant acceleration for the duration of the implosion. Applying this parabolic-trajectory model to the dashed lines of Figs. 1 and 2, one determines acceleration values in the range of $(3.4-4.2)\times10^{17}$ cm/sec^2. The agreement of the measured velocity and acceleration values with the more detailed histories of the respective computations tends to confirm our physical models for energy transport in these exploding pusher target experiments.

In conclusion, we have presented detailed measurements of the spatially and temporally resolved dynamics of laser-imploded fusion targets. These results provide the first direct measures of target implosion velocity and acceleration, and are consistent with theoretical modeling of the exploding-pusher process.

The authors wish to acknowledge the contributions of their colleagues H. G. Ahlstrom, J. H. Nuckolls, J. E. Swain, R. F. Wuerker, B. W. Weinstein, C. H. Dittmore, and J. W. Houghton.

*Work performed under the auspices of the U. S. Energy Research and Development Administration.

[1]J. Nuckolls, L. Wood, A. Thiessen, and G. Zimmerman, Nature (London) 239, 139 (1972).

[2]P. M. Cambell, G. Charatis, and G. R. Monty, Phys. Rev. Lett. 34, 74 (1975).

[3]F. Seward, J. Dent, M. Boyle, L. Koppel, T. Harper, P. Stoering, and A. Toor, Rev. Sci. Instrum. 47, 464 (1976).

[4]V. W. Slivinsky, H. G. Ahlstrom, K. G. Tirsell, J. Larsen, S. Glaros, G. Zimmerman, and H. Shay, Phys. Rev. Lett. 35, 1083 (1975).

[5]D. T. Attwood, L. W. Coleman, J. T. Larsen, and E. K. Storm, Phys. Rev. Lett. 37, 499 (1976); references to similar instruments cited therein.

[6]J. F. Holzrichter and D. R. Speck, J. Appl. Phys. 47, 2459 (1976).

[7]J. E. Swain, H. G. Ahlstrom, A. Glass, K. R. Manes, E. K. Storm, F. Rienecker, J. A. Monjes, D. E. Campbell, and L. Seppala, Bull. Am. Phys. Soc. 21, 1029 (1976), and to be published.

[8]D. T. Attwood, B. W. Weinstein, and R. F. Wuerker, "Composite X-Ray Pinholes for Time-Resolved Microphotography of Laser Compressed Targets" (to be published).

[9]The 6-μm-diam pinhole, as described in Ref. 8, is laser-drilled in a 60%-Ta_2O_5 silicate glass, which is subject to damage from the unabsorbed laser light and from general target debris.

[10]Time-integrated x-ray microphotographs for these targets do not display the familiar ring pattern (Refs. 2 and 3) associated with targets of larger radius and lower absorbed power per unit mass.

[11]J. T. Larsen, Bull. Am. Phys. Soc. 21, 1029 (1976).

Motion of Clusters on Surfaces

Uzi Landman, Elliott W. Montroll, and Michael F. Shlesinger*
Institute for Fundamental Studies, Department of Physics and Astronomy, University of Rochester, Rochester, New York 14627
(Received 5 November 1976)

A stochastic model of the diffusion of atomic clusters on crystalline surfaces, capable of treating complex systems, has been developed. Novel methods allow the analysis of diffusion data in field-free and -biased experiments. Expressions for the complete determination of parameters characterizing the individual cluster configurations from measurable quantities are derived.

The observation of the motion of atomic species on surfaces with resolution power of atomic dimensions became available only recently,[1-6] mainly through the use of field-ion-microscopy[7] (FIM) techniques. An important observation is that adatoms can form small clusters which diffuse (as exhibited on several fcc and bcc metal surfaces[2-6,8-12]) by undergoing transitions between the possible cluster configurations. The nature of the motion depends on the surface morphology [e.g., one-dimensional (1D) "channeled" diffusion of tungsten clusters on the (211) plane of W (Refs. 8–10) versus 2D diffusion of platinum clusters on the (110) plane of W (Refs. 5, 11, and 12)]. Also, under the influence of high electric fields, directional migration of clusters can be effected.[5,13]

Of basic importance in the construction and evaluation of theories of processes like thin-film

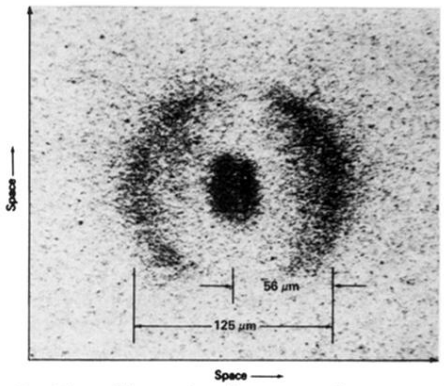

FIG. 6. Two-dimensional x-ray microscope image (time integrated) for the same target experiment described in Fig. 5.